J. Condensed Matter Nucl. Sci. 33 (2020) 1–28

Research Article

Progress Toward an Understanding of LENR–AHE Effects in Coated Constantan Wires in D_2 Atmosphere: DC/AC Voltage Stimulation

Francesco Celani [*,†], C. Lorenzetti, G. Vassallo[‡], E. Purchi, S. Fiorilla, S. Cupellini, M. Nakamura, R. Burri, P. Boccanera, P. Cerreoni and A. Spallone[§]

International Society for Condensed Matter Nuclear Science (ISCMNS_L1), Via Cavour 26, 03013 Ferentino (FR), Italy

Abstract

This paper presents a summary and some deeper details about the experiments presented at the 22nd International Conference on Condensed Matter Nuclear Science (ICCF22). It reports on the experimental study of LENR phenomena in Constantan ($Cu_{55}Ni_{44}Mn_1$) from its inception in 2011 to the most recent experiments. Using an empirical approach we identified the effect of surface modification of the Constantan wires with coatings comprised of elements that enhance the absorption behavior, and oxides with low work function for electron emission. We also explored certain geometrical arrangements of the wires such as knots and coils in order to induce local thermal gradients and predictable hot-spots. Moreover, the DC polarization of the wires by a counter-electrode proved to be a versatile approach to induce non-equilibrium conditions that are essential for Anomalous Heat Effects (AHE), especially when a dielectric barrier discharge (DBD) is produced. From the review of experiments summarized in this article, we obtain indications that the main parameter controlling the AHE is the *flux* of reactive species through the surface of the loaded material. As a consequence, all other external conditions of the reactor core (voltage–current, temperature, pressure, electric field stimulations, DC and/or AC external fields), can be seen as co-factors that enable a flux of active species through surfaces and in the bulk of the materials. Although most of the tests are in agreement with a possible flux model, some results still lack an interpretation, probably due to limits of the experimental setup.
 ISSN 2227-3123

Keywords: Anomalous Heat Excess (AHE), Cu–Ni–Mn alloy, Deuterium, Dielectric barrier discharges (DBD), Hydrogen, Low work function coatings, Nickel–Copper alloys, Nickel hydrides and deuterides

*Corresponding author. E-mail: franzcelani@libero.it.
†Also at: Ist. Naz. Fis. Nuc.-Lab. Naz. Frascati (INFN-LNF), Via E. Fermi 40, 00044 Frascati(RM), Italy.
‡Also at: DIIS, University of Palermo, 901298 Palermo (PA), Italy.
§Also at: Ist. Naz. Fis. Nuc.-Lab. Naz. Frascati (INFN-LNF), Via E. Fermi 40, 00044 Frascati(RM), Italy.

© 2020 ISCMNS. All rights reserved. ISSN 2227-3123

1. Introduction

Our group has studied Anomalous Heat Effects (AHE) in nickel–copper alloys for several years [1–10]. Apart from some initial speculation [5] one of the motivations for the choice of these materials came from the work of Romanowski [11] who showed their remarkable capability at promoting the dissociation of molecular hydrogen (H_2). Moreover we came across the work of Bruckner [12] who observed a reduction of electrical resistance of the alloys when exposed to hydrogen as well as the pioneering experiments of Ahern with Ni–Cu multilayer structures [13].

Among various Ni–Cu alloys, Constantan ($Cu_{55}Ni_{44}Mn_1$) wires became in particular the focus of our studies because of their low cost, versatility and robustness in various experimental setups. To sum up, Constantan resembles palladium (which has been more extensively studied) in that both require loading with D_2 or H_2, and conditions of *non-equilibrium* to produce AHE.

Under certain conditions indeed, absorption and/or desorption, of D (or H), are associated with exothermic phenomena exceeding by orders of magnitude the enthalpy of conventional chemical reactions.

Still, when non-equilibrium conditions are absent, AHE are either reduced or they tend to decline over time. This observation led our group to investigate ways to increase non-equilibrium conditions through years of trial and error. In a typical experiment, a 200 μm Constantan wire is oxidized by heating it in air with direct current or with a sequence of short duration, low repetition rate pulses of high peak power. These repeated oxidations create a sub-micrometric texture of oxides featuring a large surface area. The oxides are then easily reduced and the resulting porous layer enables the quick absorption of D (or H). Significant improvements in reproducibility and AHE magnitude were made by modifying this porous layer with low work function oxides [4] comprised of strontium, potassium, iron, and manganese. An SEM analysis of wires after treatment and reduction shows a sub-micrometric texture of heterogeneous composition where areas rich in nickel and copper respectively can be easily distinguished, iron and manganese instead appear in isolated islands whereas potassium and strontium oxides are uniformly distributed.

That being said, the experiments are conducted by direct constant-current heating of the wires in a D_2 atmosphere. Typically they are allowed to saturate at a pressure of 2 bar for a few days at a temperature between 300 and 500°C, then the pressure is gradually reduced below 100 mbar. In general, AHE occurs if a series of conditions previously reported [3,4] are met. AHE proves indeed to be *correlated with the amount of absorbed deuterium as well as with the presence of non-equilibrium conditions that we speculate promote a flux* [14] *or migration of active species at the interfaces of the spongy wire*.

Initially, changes in pressure, temperature, voltage, current, and the arrangement of the wires showing thermal gradients (i.e. hot spots), were introduced with a certain degree of success [6,12].

Quite interestingly the authors also found a remarkable empirical association among the thermionic emission of the wires and the occurrence and intensity of AHE [6]. Despite a lack of a clear mechanism, this peculiar correlation quickly became the focus of much experimental work. This turned our attention to electric stimuli such as the introduction of a voltage with a second wire acting as counter electrode, and even a low frequency alternating polarization (50 Hz). Afterward, a new setup was designed to isolate and explicate the effects of the thermionic emission from the hot wires and electric stimuli, hence in the most recent experiments, strong thermal gradients were avoided with respect to the knotted wire design described in [8]. In fact, above a certain temperature, thermal gradients, although particularly effective at increasing AHE magnitude, proved to be insufficient at obtaining a longlasting effect without the use of additional stimuli (changes in pressure, current, etc.).

In general we face the need to maximize the thermionic emission of the wires as well as their deuterium loading. Unfortunately these two parameters require opposite operating conditions: thermionic emission increases at low pressures, but low pressures cause the wire to unload (i.e. it allows excessive release of stored deuterium) hence leading invariably to the suppression of AHE after some time [10]. This issue was initially tackled by conducting experiments at a pressure that could prevent excessive release of deuterium from the wires while still allowing electrons to be

emitted from the Constantan wires coated with low work function elements. Also, the distance between the active wire and the counter electrode was kept as low as practically possible to promote electron emission without using an excessive voltage which could lead to localized arcs.

Such conditions are in agreement with the Child-Langmuir equation for the transport of electrons in vacuum [15,16]. Although to date a working model is not available, our speculations include a role for ionized deuterium and its interaction with electrons [9,10].

2. Chronology of the Experiments with Constantan Wires

Chronology of the experiments with Constantan wires is shown in Table 1 and the Experimental Design is shown in Fig. 1.

3. Wire Treatment and Effect of Diameter and Length on AHE

To prepare the wires, including the oxidation and coating steps, we used the same procedures described in previous papers [4]. We would like to emphasize that thinner wires consistently provide higher AHE This was observed in several experiments where we compared 100, 200 and 350 μm wires. The AHE magnitude observed in multiple experiments seems to fit qualitatively with the ratio between the section area of the oxidized layer formed during the preparation of the wires and the area of the non-oxidized core. Figure 2 shows these ratios for wires of different diameters based on SEM observations. We think that the porous and spongy oxidized layers at sub-micrometric dimensionality, upon reduction, provides a porous region/skin which may be more receptive for deuterium (or hydrogen).

Moreover thinner wires, when heated by direct current in the reactor, feature a significantly higher current density and a larger voltage drop along their ends (similarly to NEMCA [17] or Preparata [18] effects).

Table 1. Chronology of experiments with Constantan wires.

Year	Main achievement	Reference
2011	Beginning of experiments with oxidized wires, of Nickel–Copper alloys in pure H_2, D_2 or H_2/Ar, D_2/Ar mixture atmosphere, first measures of AHE in Constantan	[1]
2013	Reproducibility of AHE occurrence enhanced after coating the wires with low work function materials (SrO) and inserting the wires in sheaths of borosilicate glass fibers	[1,2,4]
2015	AHE occurrence associated with Fe impurities on Constantan wires	[4]
	Further improvements in reproducibility after adding Fe, Mn and K to the low work function main coating of the wires	
	Observation of thermionic emission from the wires in accordance with Richardson law and related Child–Langmuir law	
2017	AHE magnitude increased through geometrical arrangements to create thermal gradients along the wires	[6]
	Air flow calorimetry introduced for better AHE measures	
2018	AHE occurrence empirically associated with thermionic emission of the wires, a counter electrode is introduced to enhance electron emission and AHE	[6–8]
2019	AHE effects stabilized (from hours to days) through high voltage and alternating current stimuli. Observation of the effect of dielectric barrier discharge on AHE occurrence and magnitude	[9,10]

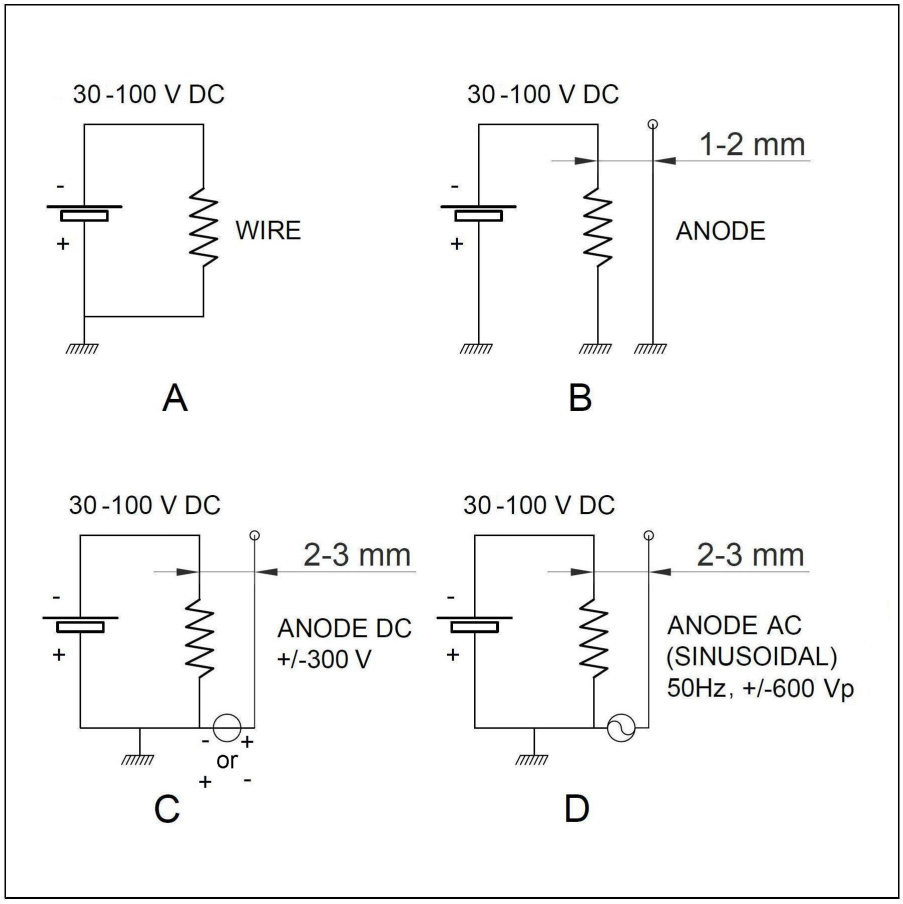

Figure 1. Evolution of the experimental set-up: Constantan wire reactor (A); grounded counter-electrode is added (B); counter-electrode is polarized with direct current (C); counter-electrode polarized with alternating current (D).

Giuliano Preparata, in particular studied the AHE generation as function of the *total voltage drop along the wire*, assuming that it may behave as if in a coherent state. The coherence phenomena and their relation to LENR, although controversial, are still the object of investigations [19].

4. Richardson and Child–Langmuir Laws

In 2014, the authors added an independent wire in close proximity to the active Constantan and observed, at high temperatures, a weak electrical current flowing when powering the first wire [4].

This current proved to be strongly related to the temperature of Constantan wire and unmistakably the consequence of thermionic emission (where the treated Constantan is a cathode and the second wire an anode), in close agreement with the Richardson law [8,9,20]. The recorded current follows a pattern in accordance with the Child–Langmuir law. Further details can be found in [15].

Later, our experiments showed that the thermionic effect and the spontaneous voltage between the two wires were

correlated to AHE occurrence. To date no clear model can explain the association of the thermionic effect and AHE occurrence, but the consistency of the relationship among the two phenomena has been confirmed in multiple experiments. Also, as mentioned above, the presence of thermal and chemical gradients is considered as being particularly relevant, especially when interpreting the large effect of knots on AHE magnitude.

5. Knots and Thermal Gradients

In 2018, mostly following a trial and error approach, attempts to further increase AHE focused on the study of different types of knots, leading eventually to the choice of the Capuchin type (see Fig. 3).

This knot design leads to several hot spots along the wire and comprises three areas characterized by a temperature difference up to several hundred degrees. The temperature difference between the external spires of the knot and the internal straight segments may also induce voltage between the spires arising from an ohmic drop along the wire, and from the different temperatures between the inner and external part of the knot.

We must emphasize that a large AHE rise was observed when introducing an extra voltage between the active wire (cathode) and a second close wire (anode) through an external power supply.

6. Coil Design

As anticipated, after the study of the wires with strong thermal gradients induced by knots, we realized they have mechanical and aging limitations, so we initiated various experiments focusing on the use of electric stimuli only. The

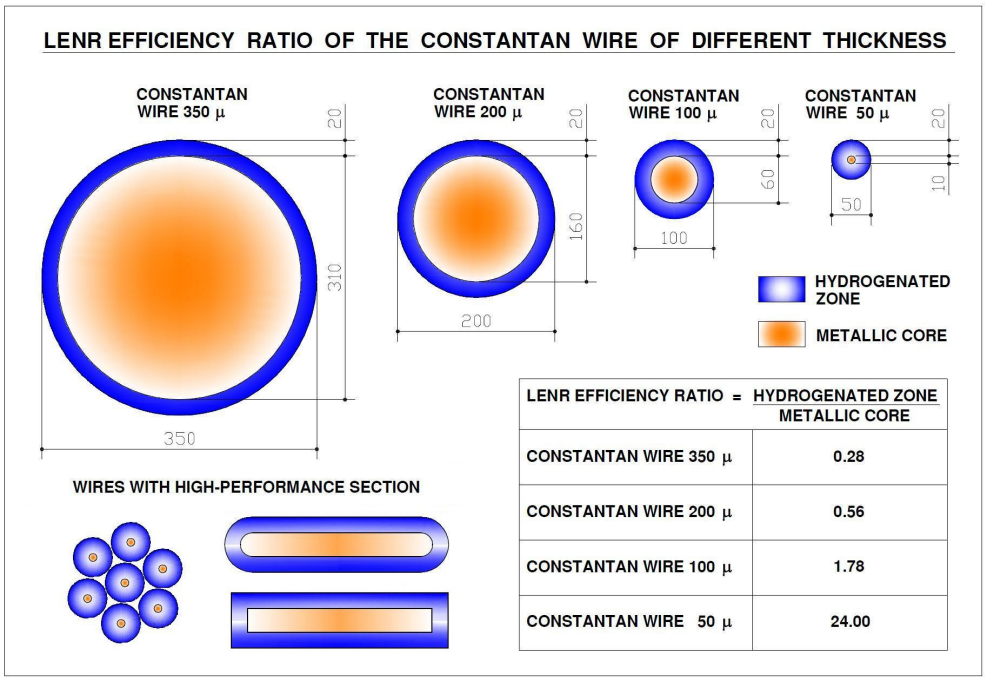

Figure 2. Section of wires of different diameter after oxidation and additional treatments. We observe the formation of a porous oxidized layer that later is reduced by deuterium. The resulting porous skin is especially prone to enhanced deuterium absorption (*blue area*). These schematic figures are based on measurements taken by Scanning Electron Microscopy. The highly loaded zone is in the range of 15–25 μm.

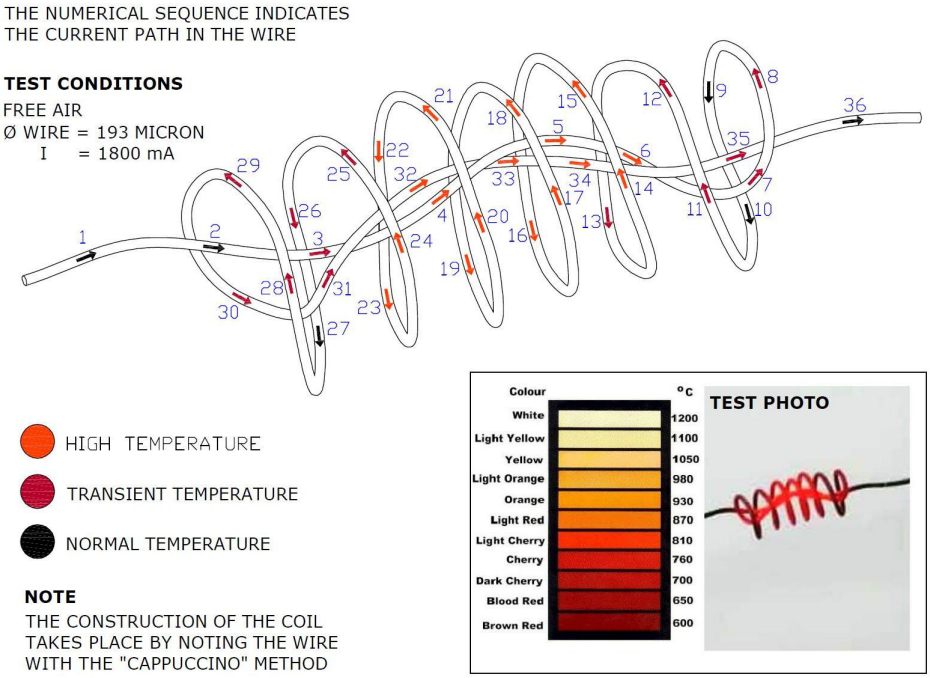

Figure 3. A knot comprised of eight loops heated in air with a direct current (Φ =193 μm, I = 1900 mA). The external diameter of the coil is 15–20 mm. Based on a color analysis, the darker area is likely to be at a temperature of <600°C, the external spires at about 800°C, while the innermost straight section may reach 1000°C. The wire used in experiments is 200 cm long and may have 4–8 knots of this type.

strong empirical association between AHE and thermionic emission guided us toward the use of a second wire with a positive polarization, to enhance electron emission from the active wire. In a more recent setup, shown in Fig. 4, a 200 μm (or 350 μm) Constantan wire is oxidized and coated with a low work function oxide (SrO). The wire is then inserted in an original sheath (made by SIGI-Favier) comprised of borosilicate glass fibers (each fiber has Φ =5 μm) tightly woven with quartz-alumina fibers (the latter to enhance the temperature resistance of the sheath). The sheath is also impregnated with the same solution of low work function elements used to treat the wires. The sheathed wire is then coiled on an iron tube insulated with a thin sheath of quartz-alumina fibers only. The Pt wire has the same geometrical configuration as the Constantan wires, except for the missing surface treatments and sheath impregnation. In this configuration the iron tube is used as a counter-electrode to study the effect of voltage bias on AHE occurrence and magnitude.

A schematic of the assembly is shown in Fig. 4.

7. Reactor Assembly

The reactor consists of a borosilicate glass tube (Schott type 3.3); dimension: Φ = 33-40 mm,L = 400 mm. A SS-304 tube (carefully cleaned to exclude sulfur), is used as central support to hold in place the coils of wires (V1, V2, V3 in Fig. 5). This tube encloses an additional thermocouple to measure the mean gas temperature inside the reactor.

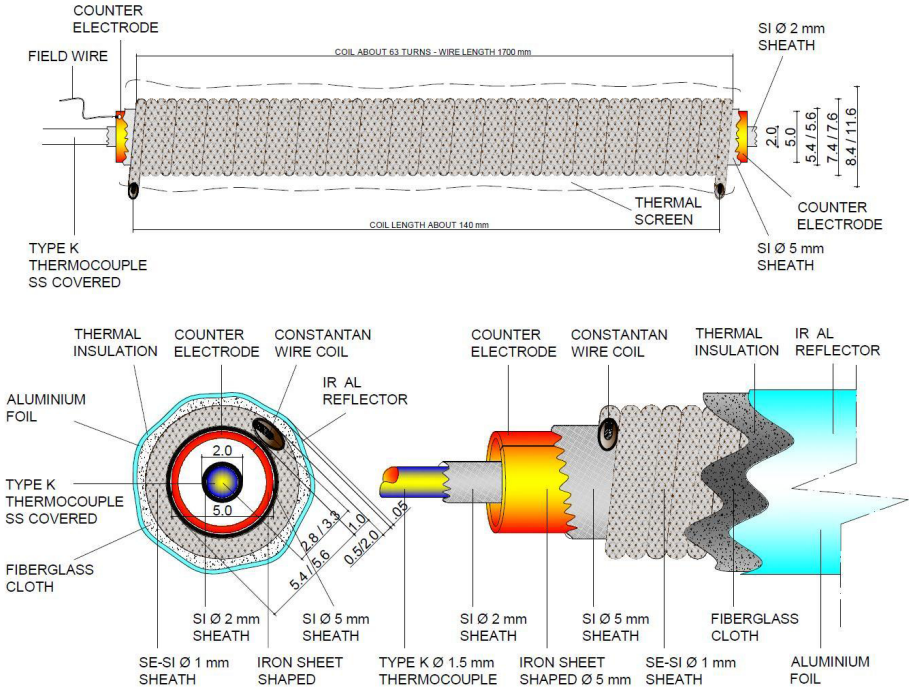

Figure 4. Details of a coil in its final assembly. The counter-electrode is a Fe tube covered by an electrical insulating, thin quartz-alumina fiber sheath. The details of construction are the same for Pt and Constantan wires. (Please note that the Constantan coils have an internal thermocouple contained in a SS tube, the internal thermocouple is not used for the platinum coil whose temperature is measured from its variation of resistance.)

On the outside of the reactor we positioned a sealed source of gamma radiation (Fig. 6) comprised of WTh2% TIG electrodes (Thoriated Tungsten alloy). This source is located inside a hermetically sealed, 2 mm thick, SS304 tube and has a nominal maximum intensity of 33 kBq. Only X-gamma radiation, specifically from thorium decay, can pass through the stainless steel tube and reactor wall to reach the Constantan wire (15 mm away from the source outer wall). In fact, the use of gamma sources is well known to facilitate electron emission as well as a trigger for avalanche ionization phenomena especially in the presence of static potential (see addendum B for further information on the source).

8. Direct Current (DC) Electric Stimuli

Wires are heated by different DC constant-currents at various power levels (usually 40–120 W). The AHE occurs usually in the range of temperatures of 650–850°C, after loading the wires at 2 bar of D_2 for 2–4 days at 300–500°C, and inducing non equilibrium conditions. This can be executed by decreasing the pressure, up to a minimum of approximately 10 mbar. In a typical experiment the AHE may last up to one day but then it slowly vanishes. This behavior may be attributed to: (a) desorption of deuterium from the wire and (b) decrease of effectiveness of the non-equilibrium conditions that may have triggered AHE release in the first instance.

To reactivate AHE release, usually, a new loading cycle at high pressure is needed.

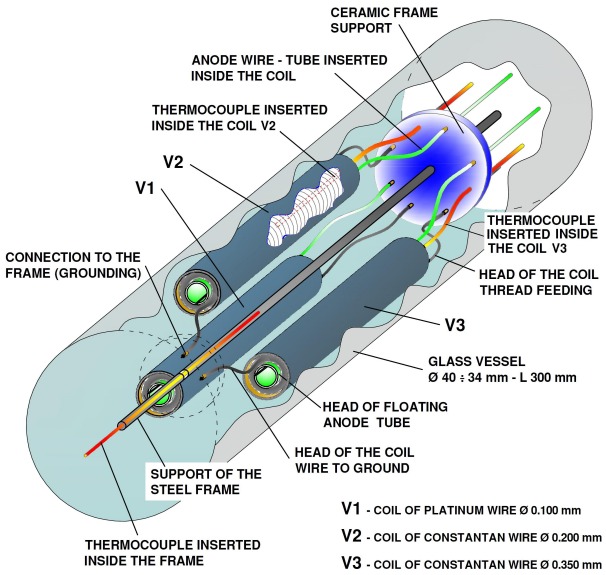

Figure 5. Assembly of the reactor including three coil cartridges, V1 is a platinum coil used mainly for calibrations, V2 and V3 are two active coils comprised of treated Constantan wires. The V1 temperature is measured using its variation of resistance; the V2 and V3 coil temperatures are measured by thermocouples inside the coil. An additional thermocouple (*in red*) is inside a SS tube used as support for the steel frame holding in place the three coils. This thermocouple is used to estimate the mean internal temperature of the reactor. All the thermocouples are type K, SS screened; insulated by MgO: 1200°C maximum temperature.

In the last two years, we have found that a practical approach to reducing the AHE decline and increasing the AHE magnitude is the application of a voltage (bias) between the wire and a counter electrode. As already mentioned, we observed an AHE increase by applying a static positive polarization to the Constantan wire (cathode); later we also witnessed an effect with a negative polarization.

This led eventually to the choice of an AC stimulus (Fig. 1D) between the Constantan wire and the counter electrode. Figure 5 shows the electrical connections of each coil used in the latest reactor assembly. The wires are inserted in theirs sheaths (Figs. 4 and 5) and then wound on a tubular Fe support, macroscopically insulated by a porous and thin-wall sheath of quartz-alumina fibers.

The excitation voltage is applied between the main wire (which is always heated by direct current, whether it is Pt or Constantan) and the Fe counter-electrode.

The deuterium loading of the wires is monitored continuously by a dedicated circuit shown in Fig. 7. This allows us to measure the ratio between the actual resistance (R) of the wire and its resistance (R_0) before the first deuterium loading. The circuitry is based on JFET J511 (Constant Current silicon diode, three in parallel, each providing 4.7 mA of current) and operates at low power only.

The same approach is used also when higher power is applied to the wires (up to 120 W in some experiments, up to 3 A of current with a 350 μm wire). Both circuits are operated in parallel, self-decoupled by a network of high voltage diodes, as a sum node. To put it in a few words, when Constantan absorbs hydrogen or deuterium, the wire resistance decreases; the larger the decrease, the larger is the loading.

A second section is designed for the low power (0.1–5 W, $\pm 600\ V_p$), used to feed the alternating current excitation

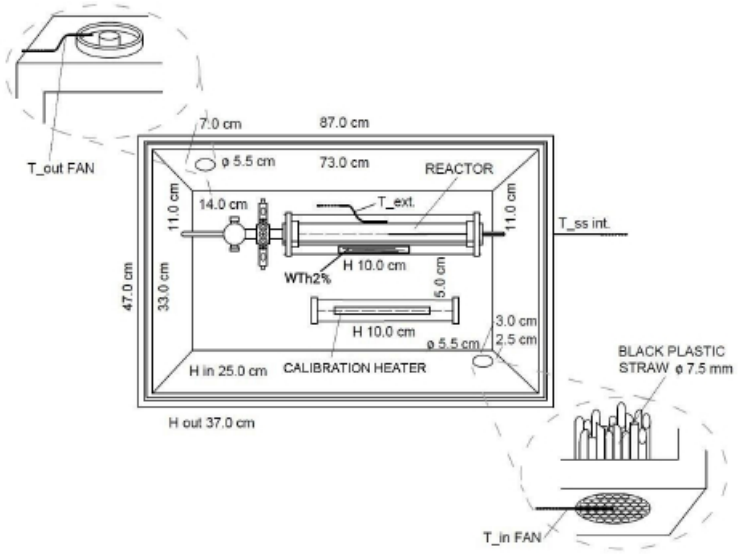

Figure 6. Scheme of the calorimeter, which is comprised of the reactor and calibration heater. Coil cartridges (V1, V2, and V3) as per Fig. 5 are not shown. T_ext is a thermocouple used to monitor the temperature of the reactor external wall, while T_ss is the thermocouple used to measure the reactor mean internal temperature.

(AC). It includes several protection networks (based on back to back 150 V, 5 W Zener diodes shown in Fig. 7) put on each end of the active wires (Constantan and Pt) in parallel to the coaxial connector, to avoid potential failures, to the main power supply and acquisition system, due to couplings of the high voltage AC pulses. The $\pm 600\ V_{\mathrm{p}}$ are applied to promote both Richardson–Child–Langmuir (only the positive region of the wave, lower pressures) and Paschen regimes (corresponding to a pressure of 30–40 mbar in our geometrical configuration, featuring a distance of 2–3 mm between the electrodes). The rationale of the circuitry is keeping the wires always polarized by a proper amount of

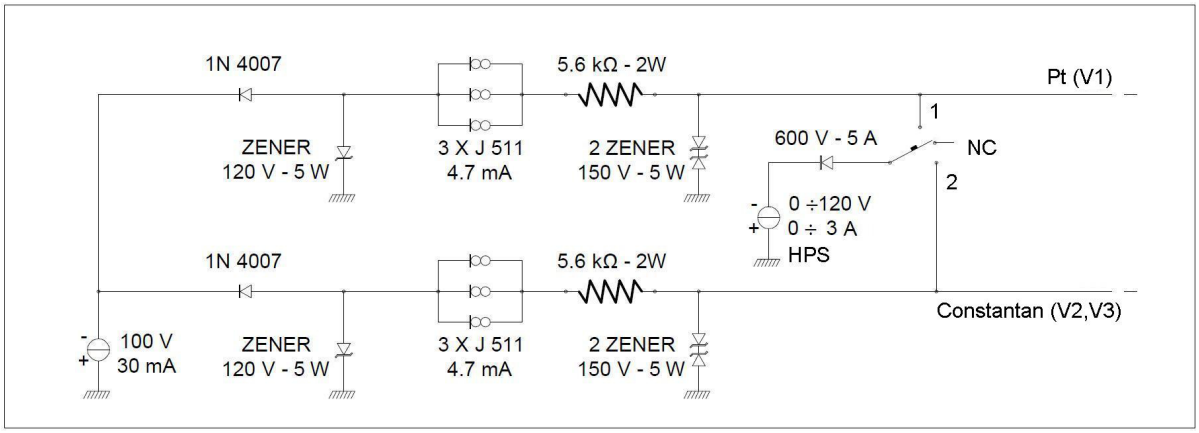

Figure 7. Scheme for the circuitry adopted for R/R_0 measurements.

current, this in order to measure the temperature of platinum wire (V1) and Resistance Ratio (i.e. R/R_0) in the case of Constantans (coils V2 and V3).

This reduction of resistance, with respect to the value of Constantan before absorption (R_0), is likely related to the amount of H (or D) absorbed by the wire similarly to what observed with palladium above a certain loading [21]. That being said, a precise correlation among absorbed H (D) and resistance is not yet available nor fully understood for the case of Constantan wires (which as shown in Fig. 2 show nonhomogeneous absorption across their section).

Also, the minimum current injected to maintain the wires polarization, is about 14 mA and is feed by the three constant current diodes (CCD) in parallel (J511 in the scheme of Fig. 7). When higher current needs to be injected, a High Power Supply is used (HPS: –120 V, 0–3 A). Appropriate high voltage diodes prevent the current from going back to the low power supply section (when the high current path is active). The output of HPS has three positions: 1, connected to Pt (connector V1); 2, connected to the Constantan (connector V2 or V3); three unconnected (NC).

Among others, some explorative tests were made with: (a) unipolar half-wave, positive or negative pulses (see Appendix A for the circuits used in this case). The Richardson regime, with the related Child–Langmuir current, occurs at a rather low pressure and the emission intensity of electrons at the surface of the material depends both on the temperature and the value of the work function of the material. We recall that the electrons boil-off at the *surface* of the low work function materials: they create a spatial-charge localized in close proximity of the surface until some external field of positive polarization is applied removing them [3,6,20].

Concerning the *Paschen* regime, with respect to the original formula developed in 1889 by Friedrich Paschen [22–28] in free air and parallel plates, we must consider that the use of low work function materials and the presence of the thoriated tungsten source outside the reactor is likely to influence the discharge initiation.

Under these conditions, we think that the breakdown voltage would be significantly reduced.

9. Alternating Current Electric Stimuli

The AC circuitry that generates 1200 $V_{\rm pp}$ was applied to the counter-electrode. It is based on two 50 Hz, multiple output transformers in cascade. This allows us to increase the 230 $V_{\rm rms}$ (i.e. 324 V_p) of the line to 610 $V_{\rm p}$ as measured by oscilloscope.

The current needed for the excitation is rather low, with a limit at 60 mA due to a 10 kΩ limiting resistor. Usually the current does not exceed 10–20 mA because the triggering voltage of the Paschen effect is approximately 400–500 V and RMS values up to 5–6 mA, as measured by a Fluke 187 multimeter (BW=100 kHz). The RMS voltage is in the range 250–280 V, as measured by a Tektronix DMM916 multimeter (BW=20 kHz). For higher accuracy, and better understanding of waveforms, especially the higher frequency components, the signal at the end of a 10 kΩ resistor is sent to a Fluke 198C Digital Scope (BW=100 MHz). Some of the most significant operating situations are reported in Figs. 10–12.

Figure 10 shows in particular a typical waveform corresponding to a limited coupling between the counter electrode and the active wire (under high pressure or pure deuterium). As deduced from Fig. 8, the addition of Ar is able to reduce significantly the voltage needed to initiate a discharge. Figure 11 shows instead the waveform observed using a 1:1 molar mixture of Ar and D_2 at a pressure compatible with discharge occurrence (as per Fig. 8). In these conditions AHE is substantially increased compared to the case presented in Fig. 10.

Finally Fig. 12 shows the remarkable occurrence of a dielectric barrier discharge, and it is definitely the most effective at producing AHE. However, it is rather difficult to maintain and the materials (especially the insulating sheaths) shows signs of degradation after few hours, probably due to arcing. According to the literature, an increase of frequency (from present 50 Hz up to values of 10–40 kHz) and optimization of tension and wave form, could limit the drawback and it is currently under investigation.

That being said, due to the high voltage needed for AC excitation, the injection circuitry and measuring set-up

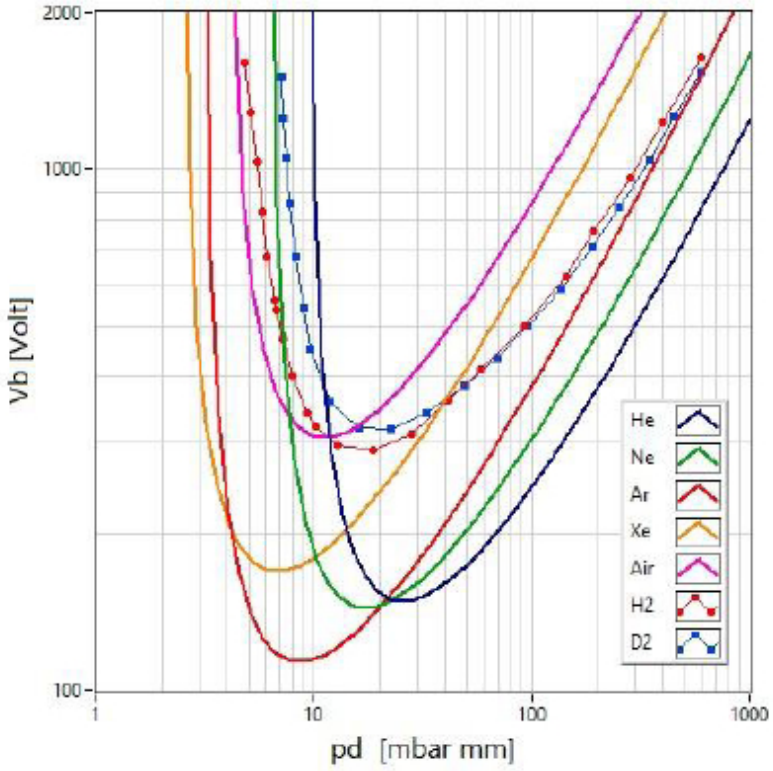

Figure 8. Direct current breakdown tension (V_b) of several gases versus pressure and distance between electrodes (p*d) [29]. The addition of argon to deuterium clearly enables discharges at lower tension.

is currently being improved. This is in order to reduce the value of the 10 kΩ limiting resistor and to boost the peak current at high voltage. Non-linear circuitry with overall improved high frequency performance, is under consideration.

Some of the waveforms observed by the oscilloscope are reported in Figs. 10–12. Curves in Fig 12 seem to be associated with the highest AHE. In these conditions a dielectric barrier discharge is clearly occurring.

10. Calorimetry

AHE occurrence was studied using air-flow calorimetry.

The calorimeter consists of an insulated case made of double walls (6.5 cm in total), thick polystyrene whose each internal surface is covered with multiple reflective thin aluminum foil. This apparatus is calibrated using a Nichrome heater inside the calorimeter case or a platinum wire coil inside the reactor (V1 in Fig. 5) under inert gas (He).

The Ni–Cr heater is contained in a borosilicate tube having dimensions similar to the active reactor. Both the heater and the reactor are placed in close proximity. They are covered by several corrugated layers of 40 μm thick Al foils with one black side. An overview of the assembly is shown in Fig. 6. The fan is 5 cm wide, operates in suction mode, and has a nominal air flow of 4.445 l/s at normal pressure and temperature (NPT), and it rotates at 75 Hz. Its revolution rate is monitored, and the measurement is logged in the acquisition system. The overall average coefficient of heat exchange during calibrations (e.g. in the restricted power range of 90–110 W) with the Ni–Cr heater or platinum wire is

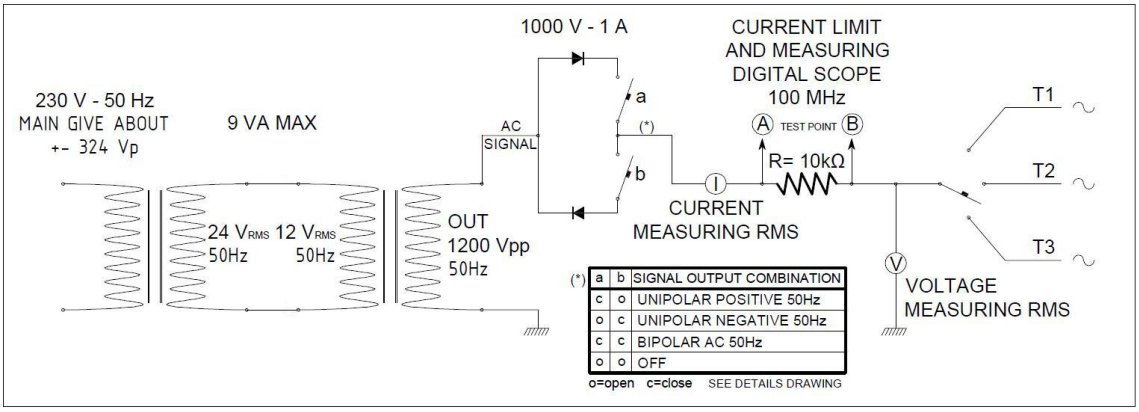

Figure 9. Scheme of the high voltage-low current circuitry adopted for AC excitation. The R limit and current measuring resistance usually has a value of 10 kΩ (T1, T2, and T3 refer to the counter electrodes of each coil which is the iron tube shown in Fig. 4).

approximately 0.20°C/W and is consistent with the values of air flow, density, pressure and air humidity (which is kept almost stable at 45–55% of RH by the air conditioning system of the laboratory) and heat capacity in the range of air temperature inside the calorimeter (20–60°C). Precautions to increase internal air turbulence are also taken to prevent air stratification which could affect the measures. A selection of over 80 tests are reported in Table 2, Appendix B.

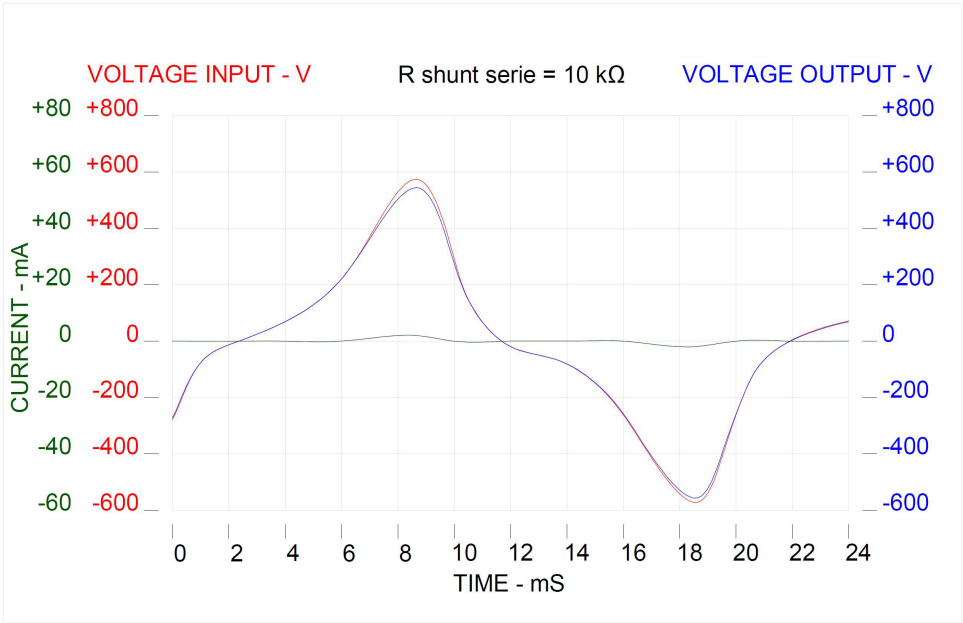

Figure 10. Voltage drop along the limiting-measuring resistor of 10 kΩ. Red is at test point **A**, blue at test point **B**. Current is the green color line. Typical waveforms in mild condition of excitation, i.e. not Dielectric Barrier Discharge (DBD) conditions. Even the Paschen regime (starting from about 400 V) looks self-quenched, perhaps due to the excessive value of the resistance (10 kΩ resistor in Fig. 10).

AHE is estimated as follows:

$$A1 = \frac{T_{\text{out}} - T_{\text{in}}}{P_{\text{in}}} \, (^{\circ}\text{C/W}) \text{ Calibration values}, \tag{1a}$$

$$A2 = \frac{T_{\text{out}} - T_{\text{in}}}{P_{\text{in}}} \, (^{\circ}\text{C/W}) \text{ Active wire values}, \tag{1b}$$

$$\text{AHE} = \frac{A2 - A1}{A1} \, P_{\text{in}} \, (W) \, , \tag{1c}$$

where T_{out} and T_{in} are the air temperatures measured at the outlet and inlet of the calorimeter, respectively, as shown in Fig. 6.

Further details on the adopted calorimetric technique can be found on the paper summarizing the presentation at ICCF21[5,6].

11. Results

In a particularly impressive experiment, 18 W of AHE were observed for an input power of 99.7 W (line #38 of Table 2 in Appendix B), recorded when using a 200 μm wire (coil V2 in Fig. 2) at a temperature of 716°C. The counter-electrode excitation consists of +270 V bias and 3 mA current, the behavior of R/R_0 was oscillating over time. The effect lasted over 5 h.

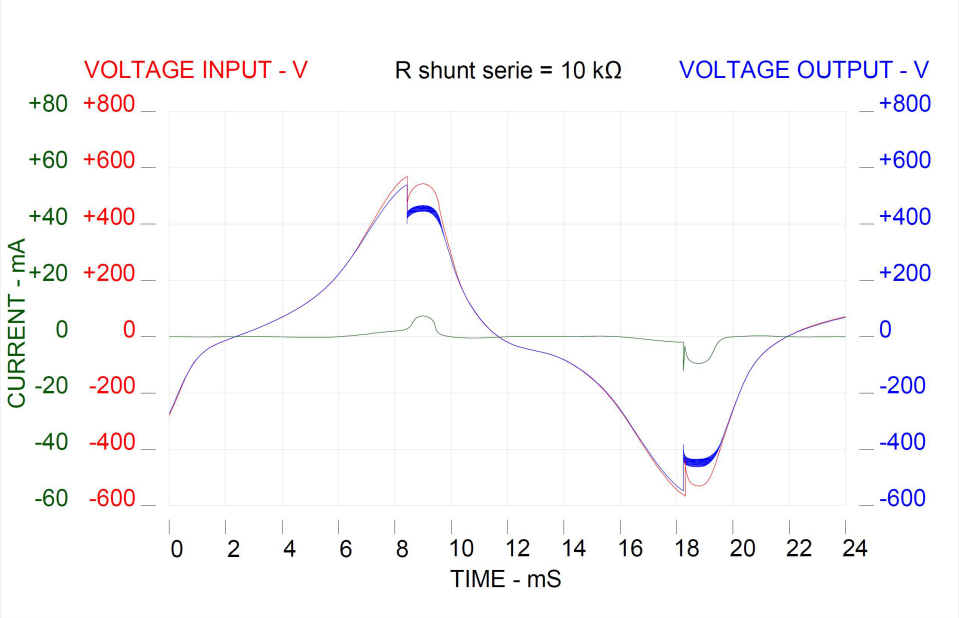

Figure 11. Similar to the case of Fig. 10 but with larger current. The current starts at a voltage value close to 400 V, as expected according to the threshold voltage of the gas involved.

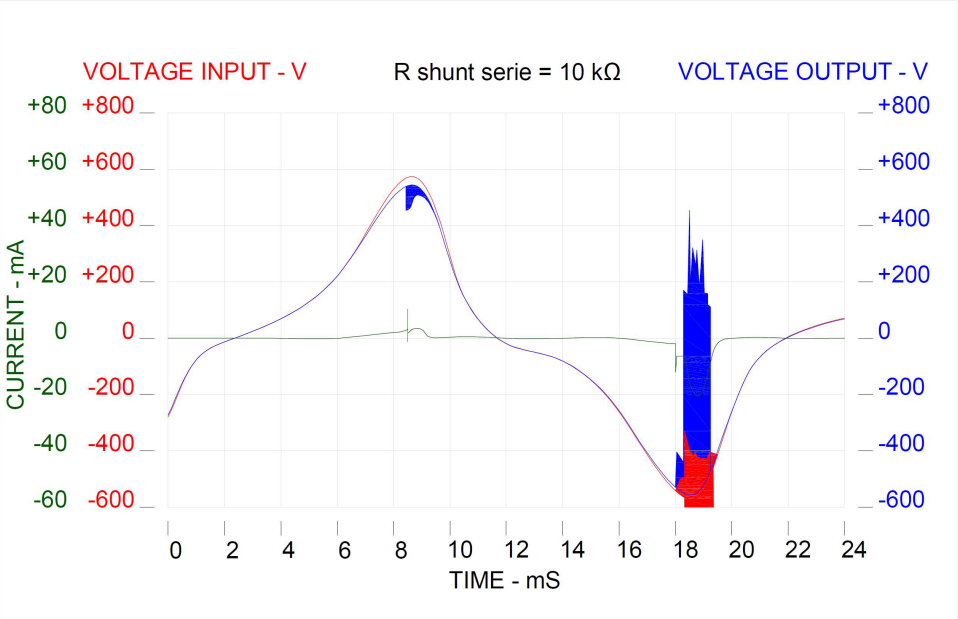

Figure 12. Typical waveform that seems to be the most efficient to increase the AHE.

Afterward AHE decreased to 9.5 W (line #39), perhaps due to air intake from a leak. In fact, the pressure increased from about 300 up to about 316 mbar. Anyway, the effect had a remarkable time span of over 15 h. When the polarity was changed from positive to negative (line #40), AHE decreased from 9.5 to 7.4 W. The shift (line #41) from unipolar negative to bipolar oscillation ($\pm$600 V_p, 50 Hz) increased AHE from previous 7.4 to 10.7 W, the effect lasted about 4 h. Reducing the pressure from 341 to 98 mbar (line #42) the effect increased from 10.7 to 14.5 W, always under AC oscillation and current (rms value) of 2–3 mA. The effect lasted 4 h. After the interruption of the AC stimulus (line #43) leakage was observed, causing a pressure increase from 98 to 250 mbar, this was followed by a reduction of AHE from 14.5 to 2.4 W. AHE slowly vanished following stabilization of R/R_0 (that was unstable and oscillating proportionately to AHE).

When AC oscillation (line #44) was resumed at a constant pressure of 250 mbar, AHE rise again, from 2.4 to 9.2 W. In general, much lower AHE values were observed when using the larger diameter wire coil V3 (350 μm). Eventually the only way to recover large values of AHE (i.e. 14.4 W, line #59), was to power 200 μm wire (V2) add some Ar to the gas mixture, keep the pressure relatively low (36 mbar), and use AC excitation to the counter electrode.

12. Conclusions

From the collected data the following conclusions can be drawn.

(a) The AHE occurrence is correlated with fast loading or unloading of the wire. In the case of unloading however, after a short time, the AHE vanishes.
(b) When loading/unloading occurs slowly, AHE is significantly reduced.
(c) A state of oscillation seems to be the most efficient since it produces AHE for a longer time with respect to fast loading or unloading (especially when a dielectric barrier discharge occurs).

(d) Loading and unloading occurrence, as assumed from R/R_0 and variation in reactor pressure, strongly support the key role of deuterium flux (see [14] for a definition of flux).

There are additional external conditions, such as high temperature, low pressure, purity of the gas that facilitate the AHE. In any case, after some time, even the optimal conditions described above are not sufficient to maintain AHE release. That being said, the major finding we would like to emphasize is the ability of the counter-electrode stimulus to keep the AHE active for longer times, perhaps indefinitely.

Also, the role of non-equilibrium conditions and flux were suggested by several researchers [30–38] since the beginning of Cold Fusion experiments. Convincing proofs being said, the set of experiments summarized in Table 2 of the present work consistently shows a strong correlation between a change in loading/pressure and the occurrence of AHE, hence providing a strong support to the flux model or hypothesis. Also, although most of the tests here described are in agreement with the flux model, some results are still difficult to interpret. We think that this could be due to accidental contamination of the deuterium due to an insufficiently air-tight glass reactor, especially at high temperature and low pressure.

Moreover, a critical analysis of the data collected in Table 2 (Appendix B) allows us to highlight a series of observations or possible generalizations on the best conditions enabling AHE release for the selected reactor geometry:

(1) Temperature must be as high as possible, provided that sintering of the spongy surface does not occur. Also, high temperature is one of the key factors for electron emission from low work function materials. We speculate that a high intensity emission may interact with deuterium (or hydrogen) leading to useful phenomena. This last statement is purely based on associations during experiments (i.e. between thermionic emission and AHE).
(2) Low pressure is useful to increase the e^- emissions. However, below a certain pressure the effect may be deleterious due to excessive deuterium release (unloading) from the wires. We would like to highlight that the occurrence of a dielectric barrier discharge (Fig. 13) is associated with a remarkably intense AHE. Although at this stage we would like to avoid venturing into a discussion of possible reaction mechanisms, we recognize some analogies with previous work and that of Randell Mills [39–42] and Jacques Dufour [43,44].
(3) The addition of low-thermal conduction noble gases (like Ar or Xe) is generally useful to increase the temperature inside the reactor core and promote the Paschen regime, when the counter-electrode has sufficiently high voltage.
(4) High DC voltages along the active wire are useful (perhaps due to NEMCA and/or Preparata effects). As a consequence, thinner wires are usually more efficient at producing AHE.
(5) The effect of AC has to be fully explored in all of its potential (varying frequency, voltage, waveform, bias, and/or asymmetries). Nevertheless, we observed an unexpected but clear correlation with the negative side of AC wave and an increase of the temperature in the reactor core when certain conditions of temperature and pressures are fulfilled. In general, AC stimuli seems to counteract the AHE decline observed in previous experimental projects.
(6) The *flux of deuterium trough the active material (Constantan)* seems to be the most important factor driving the AHE generation. Based on experimental observations, we speculate that *inducing oscillations of flux* may be the best method for triggering or increasing AHE.
(7) Contamination of the reactor atmosphere (e.g. by air and/or degradation of glassy sheaths) has a deleterious effect on AHE. Unfortunately, due to budget constraints, up to now we could not afford a Residual Gas Analyzer (RGA) placed in-line with the reactor to diagnose this problem.

Our present work aims at preventing the issues of the described experimental setup such as the frequent leakages and poor control of gas compositions. This will be achieved with a new stainless steel reactor equipped with residual gas analysis (RGA). We are also working at optimizing the electronics used as AHE stimulus and for DBD plasma

generation, as well as at finding the optimal operating conditions both with conventional high tension, medium-high frequency generators, as well with pulsed DC power supplies.

Acknowledgments

The experimental work described in this paper was presented at ICCF22 Conference (Assisi, September 8–13, 2019). This work was carried out at INFN-LNF while some trials were conducted at the premises of a Metallurgical Company of North Eastern-Italy with independent instruments and personnel. This Company has also has provided some financial support since 2011. SIGI (Società Italiana Guaine Isolanti) Favier, France, designed and produced dedicated glass fiber sheaths in close collaboration with the above-mentioned Metallurgical Company. From October 2017 Lega Nord, an important political Group in Italy, enabled the continuation of F. Celani's experiments in the Frascati Laboratory of INFN. Special thanks to Francesco Malagoli, Filippo Panini, Paolo Varini. All have followed LENR development for many years, in line with a political program focused on the protection of the environment. Antonino Cataldo and Stefano Bellucci (NEXT collaboration) performed SEM and EDX analysis at INFN-LNF. Some of the expenses to perform experiments and for travel and food, were supported by IFA group-Italy. We thank the Anthropocene Institute, USA (i.e. Carl Page and Frank Ling) for providing economic support so that two of our collaborators could attend the ICCF22. We thank Hideki Yoshino, CEO of Clean Planet Company, Japan, for providing economic support enabling another of our collaborators to attend the ICCF22. We are indebted to Luca Gamberale, one of the last collaborators of Prof. Giuliano Preparata still active in the LENR –AHE field, for the critical reading of our manuscript. We are also indebted to Jed Rothwell for proofreading the manuscript, for his scientific suggestions and for improving the English grammar, as he has done for several years.

References

[1] F. Celani, E.F. Marano, A. Spallone, A. Nuvoli, B. Ortenzi, S. Pella, E. Righi, G. Trenta, F. Micciulla, S. Bellucci, S. Bartalucci and M. Nakamura, Experimenal results on sub-micro structured Cu–Ni alloys under high temperatures hydrogen/deuterium interactions, *Chem Material Res* **3** (3) (2013) 25–76.

[2] F. Celani, E.F. Marano, B. Ortenzi, S. Pella, S. Bartalucci and S.B. F. Micciulla, Cu–Ni–Mn Alloy wires, with improved submicrometric surfaces, used as LENR device by new transparent, dissipation-type calorimeter, *J. Condensed Matter Nucl. Sci.* **13** (2014) 56–67.

[3] F. Celani, G. Vassallo, E. Purchi, S. Fiorilla, L. Notargiacomo, C. Lorenzetti, A. Calaon, B. Ortenzi, A. Spallone, M. Nakamura, A. Nuvoli, P. Cirilli, P. Boccanera and S. Pella, Improved stability and performance of surface-modified Constantan wires, by chemical additions and unconventional geometrical structures, *J. Condensed Matter Nucl. Sci.* **27** (2018) 9–21.

[4] F. Celani, A. Spallone, B. Ortenzi, P.S, E. Purchi, F. Santandrea, S. Fiorilla, A. Nuvoli, M. Nakamura, P. Cirilli, P. Boccanera and L. Notargiacomo, Observation of macroscopic current and thermal anomalies, at high temperatures, by hetero-structures in thin and long constantan wires under H_2 gas, *J. Condensed Matter Nucl. Sci.* **19** (2016) 29–45.

[5] F. Celani, C. Lorenzetti, L. Notargiacomo, E. Purchi, G. Vassallo, S. Fiorilla, B. Ortensi, M. Nakamura, A. Spallone, P. Boccanera, S. Cupellini and A. Nuvoli, LENR phenomena in Constantan; a steady progress toward practical applications: observation of Zener-like behaviour, in air atmosphere, of Constantan submicrometric wires after D_2–Xe loading–deloading and related AHE, in *12th Int Workshop on Anomalies in Hydrogen Loaded Metals*, Asti, 2017.

[6] F. Celani, B. Ortenzi, A. Spallone, C. Lorenzetti, E. Purchi, S. Fiorilla, S. Cupellini, M. Nakamura, P. Boccanera, L. Notargiacomo, G. Vassallo and R. Burri, Steps to Identify main parameters for AHE generation in sub-micrometric materials: measurements by isoperibolic and air-flow calorimetry, *J. Condensed Matter Nucl. Sci.* **29** (2019) 52–74.

[7] F. Celani and C. Lorenzetti (Eds.), Electrically induced anomalous thermal phenomena in nanostructured wires, in *Cold Fusion*, Chap 7, Elsevier, Amsterdam, 2020, pp. 101–113.

[8] F. Celani, C. Lorenzetti, G. Vassallo, E. Purchi, S. Fiorilla, S. Cupellini, M. Nakamura, P. Boccanera, R. Burri, B. Ortenzi, A. Spallone and P. Cerreoni, First evaluation of coated Constantan wires comprising Capuchin knots to increase anomalous heat and reduce input power at high temperatures, *J. Condensed Matter Nucl. Sci.* **30** (2020) 25–35.

[9] F. Celani, C. Lorenzetti, G. Vassallo, E. Purchi, S. Fiorilla, S. Cupellini, M. Nakamura, P. Boccanera, R. Burri, P. Cerreoni and A. Spallone, Effects of super-Capuchin knot geometry, and additional electric fields, on hydrogen/deuterium absorption: related AHE on long and thin Constantan wires with sub-micrometric surfaces at high temperatures, in *2019 LANR/CF Colloquium at MIT-USA*, Cambridge, MA 02139 (USA), March 23–24, 2019.

[10] F. Celani, C. Lorenzetti, G. Vassallo, E. Purchi, S. Fiorilla, S. Cupellini, M. Nakamura, P. Cerreoni, P. Boccanera, R. Burri and A. Spallone, Unexpected effects due to voltage waveform at anode, in gaseous LENR experiments based on sub-micrometric surface coated Constantan wires., in *Terzo Convegno Assisi nel Vento, Domus Laetitiae*, Assisi (PG), Italy, May 17–19, 2019.

[11] S. Romanowski, W. M. Bartczak and R. Wesołkowski, Density functional calculations of the hydrogen adsorption on transition metals and their alloys. an application to catalysis, *Langmuir* **15** (18) (1999) 5773.

[12] W. Brückner, S. Baunack, G. Reiss, G. Leitner and T. Knuth, Oxidation behavior of Cu–Ni(Mn) (constantan) films, *Thin Solid Films* **258** (12) (1995) 252.

[13] B.S. Ahern, K.H. Johnson and H.R. Clark, Method of maximizing anharmonic oscillations in deuterated alloys. Patent US5411654A, 1995.

[14] D. Ugura, A.J. Storm and R. Verberk, Quantification of the atomic hydrogen flux as a function of filament temperature and H_2 flow rate, *J Vacuum Sci. Technol* **30** (3) (2012) 1–6.

[15] K. Jensen, *Introduction to the Physics of Electron Emission*, *Child–Langmuir Law*, Chap. 16, Wiley 2017.

[16] Y.L.Y Lau, Electron emission: from the Fowler–Nordheim relation to the Child–Langmuir law, *Phys Plasmas* **1** (1994) 2082–2085.

[17] C.G. Vayenas, S. Bebelis, I.V. Yentekakis, S. Neophytides and J. Yi, Ion spillover as the origin of the NEMCA effect, *Studies in Surface Science and Catalysis* **77** (1993) 111–116.

[18] M. Cola, E.d. Giudice, A.D. Ninno and G. Preparata, A Simple Model of the Cohn-Aharonov Effect in a Peculiar Electrolytic Configuration, Vol. 70, Lerici (SP)-Italy, SIF Bologna, 2000, pp. 349–358.

[19] Luca Gamberale, Dynamical realization of coherent structures in condensed matter, in *Invited paper at IWAHLM13, October 5–8, 2018*, Greccio (RI)-Italy, 2018.

[20] O.W. Richardson, Thermionic Phenomena and the Laws which Govern Them. Nobel lecture, 1929.

[21] Y. Sakamoto, K. Takai, I. Takashima and M. Imada, Electrical resistance measurements as a function of composition of palladium–hydrogen(deuterium) systems by a gas phase method, *J Phys.: Condensed Matter* **8** (19) (1996) 3399–3411.

[22] F. Paschen, Ueber die zum Funkenübergang in Luft, Wasserstoff und Kohlensäure bei verschiedenen Drucken erforderliche Potentialdifferenz, *Annalen der Physik* **273** (5) (1889) 69– 75.

[23] D. Marić, M. Savić, J. Sivoš, N. Škoro, M. Radmilović-Radjenović, G. Malović and Z. Petrović, Gas breakdown and secondary electron yields, *Eur. Phys. J.* D **68** 155 (2014) 1–7.

[24] L.F. Berzak, S.E. Dorfman and J. Smith, *Paschen's Law in Air and Noble Gases*, Berkley, USA, 2006, pp.1–14.

[25] E.M. Bazelyan and Y.P. Raizer, *Spark Discharge*, CRC Press, Boca Raton, FL, USA, 1998, 1998.

[26] I. Donko and Z. Korolov, Breakdown in hydrogen and deuterium gases in static and radiofrequency, *Phys. Plasmas* **22** (9)(2015).

[27] M.W. Childs, Ion generator apparatus, United States Patent US10398015B2, 27 8 (2019).

[28] D. Fisher and J.d. Bitetto, Townsend ionization coefficients and uniform field breakdown, *Phys. Rev.* **104** (1956) 1213.

[29] M.A. Lieberman and A.J. Lichtenberg, in *Principles of Plasma Discharges and Materials*, Vol. 1, 2nd Edn, Wiley Blackwell, 2005, p. 700.

[30] F. Celani, Talk at the first workshop on cold nuclear fusion, in *Summary by Richard L. Garwin, Nature* **338** (1989) 616–617 *https://doi.org/10.1038/33861*, E. Majorana Centre for Scientific Culture, Erice (Italy), 1989.

[31] M. Swartz, Quasi-one-dimensional model of electrochemical loading of isotopic fuel into a metal, *Fusion Technol.* **22** (2) (1992) 296–300.

[32] G.C. Fralick, A.J. Decker and J.W. Blue, Results of an attempt to measure increased rates of the reaction $D_2 + D_2$ yields He-3 + n in a nonelectrochemical cold fusion experiment, NASA-TM-102430, E-5198, NAS 1.15:102430 , Cleveland, 1989.

[33] Y. Arata and Y.C. Zhang, Reproducible cold fusion reaction using a complex cathode, *Fusion Technol* **22** (2) (1992) 287–295.

[34] Y. Iwamura, T. Itoh and M. Sakano, Nuclear products and their time dependence induced by continuous diffusion of deuterium through multi-layer palladium containing low work function material, in *8th Int Conf Cold Fusion*, Lerici (La

Spezia),2000.
[35] M.C.H. McKubre, S. Crouch-Baker, A.M. Riley, S.I. Smedley and F.L. Tanzella, Excess power observations in electrochemical studies of the D/Pd system; the influence of loading, in *Frontier of Cold Fusion, Proc. ICCF3 Nagoya*, 1992.
[36] Y. Iwamura, T. Itoh, M. Sakano, S. Sakai and S. Kuribayashi, Low energy nuclear transmutation in condensed matter induced by D_2 gas permeation through Pd complexes: correlation between deuterium flux and nuclear products, in *Proc. of ICCF10, Condensed Matter Nuclear Science*, Cambridge, MA, 2006.
[37] Y. Iwamura, T. Itoh and N. Gotoh, Characteristic X-ray and neutron emission from electrochemically deuterated palladium, in *Proc. 5th Int. Conf. Cold Fusion, Monte Carlo* , Monaco, 1995.
[38] T.O. Passell, Use of helium production to screen glow discharges for low energy nuclear reactions (LENR), in *American Physical Society. APS March Meeting 2011.* March 21–25, 2011, Abstract ID Y33.008.
[39] R.L. Mills, W.R. Good, J. Phillips and A.I. Popov, Lower-energy hydrogen methods and structures, Patent US6024935A, 1997.
[40] R.L. Mills and P. Ray, Spectral emFractional quantum energy levels of atomic hydrogen from a helium–hydrogen plasma and the implications for dark matter, *Int. J. Hydrogen Energy* **27**(3) (2002) 301–322.
[41] R.L. Mills, P.C. Ray, M. Nansteel, X. Chen, R.M. Mayo, J. He and B. Dhandapani, Comparison of excessive Balmer /spl alpha/ line broadening of inductively and capacitively coupled RF, microwave, and glow-discharge hydrogen plasmas with certain catalysts, *IEEE Trans Plasma Sci* **31** (3) (2003) 338–355.
[42] B. Holverstott, *Randell Mills and the Search for Hydrino Energy*, KRP History, 2016.
[43] J. Dufour, J. Foos and J.P. Millot, Measurement of excess energy and isotope formation in the palladium–hydrogen system, in *5th Int Conf on Cold Fusion*, Monte-Carlo, Monaco, 1995.
[44] J. Dufour, J. Foos and J.P. Millot, Excess energy in the system palladium/hydrogen isotopes. measurement of the excess energy per atom hydrogen, in *5th Int Conf on Cold Fusion*, MonteCarlo, Monaco, 1995.

Appendix A. Auxiliary Circuitry for Explorative Tests

Auxiliary circuitries were developed to study:

(A) the effects of unipolar excitation at 50 Hz, both positive and negative. Schematic shown in Fig. 13
(B) current flowing between cathode and anode. DC level at maximum allowable voltages, +-600 V. Sketch shown in Fig. 14

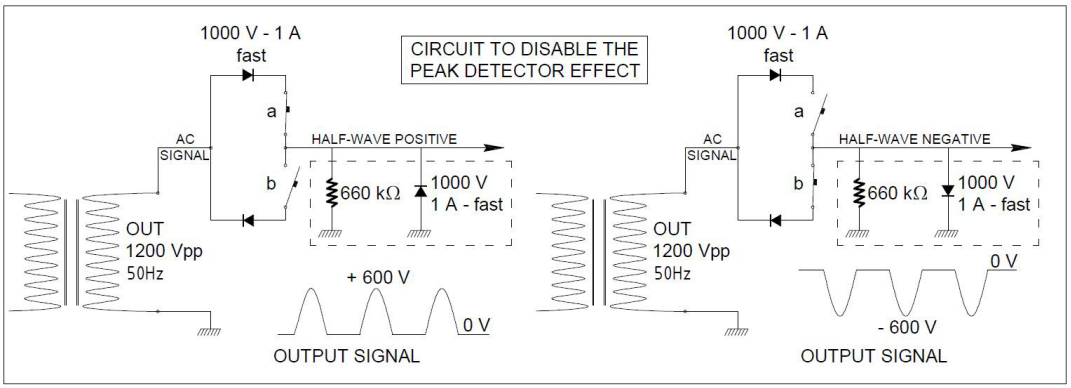

Figure 13. Circuitry to generate unipolar pulses, at 50 Hz, by a network of fast diodes and R (660 kΩ grounded). Such circuitries allowed to evaluate the effect of repetitive unipolar pulses from the point of view of AHE stimulation. The results were used to optimize the operating conditions of the reactor (gas, temperature and pressure).

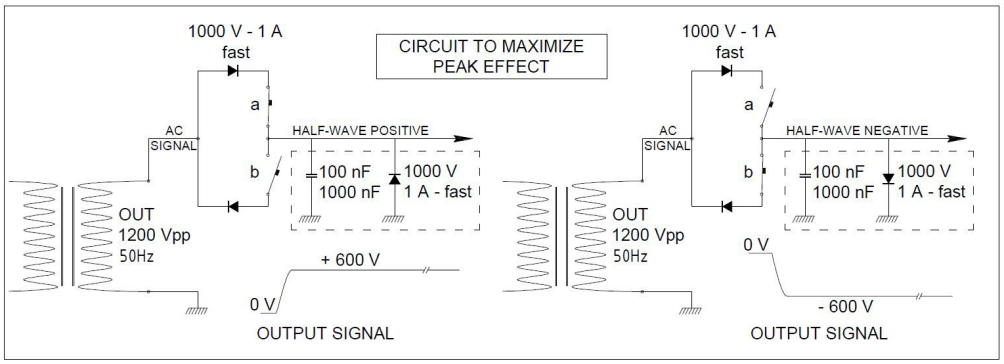

Figure 14. The simple circuitry used to generate unipolar high voltages in DC, by means of a peak detector system (D, Capacitor). Adding an ammeter between the output of the circuitry and the counter electrode it was possible to measure the current, in DC conditions, between the two wires of the reactor while changing gas, temperature and pressure.

Appendix B.

Table 2 summarizes over 80 tests performed during two months of experiments using Constantan wires, 1.7 m long, with a diameter of 200 or 350 μm. During these experiments the active wire polarity was kept negative and the extremity of each wire was grounded; the power supply was operated in the constant-current mode. The table includes the following data:

C1 Identification of the experiment, time [s] since the start of specific data logging.
C2 Wire diameter (mm).
C3 Electric input power (W), Voltage along the wire (V), Current (A).
C4 Gas type, pressure (mbar).
C5 Temperature at the core of each tube/cartridge used for the Constantan wires (inside the Fe counter-electrode); the R/R_0 value of the wire; the trend of its variation over time (reported on the last 10 ks) as observed in the plot of raw data.

The wire loading during the experiments was classified, as follows:

C5.1 Increase of Loading (IL), corresponds to a R/R_0 decrease; it can be Slow (S) or Fast (F) (e.g. IL_S means slow increase of loading).
C5.2 Decrease of Loading (DL), corresponds to a R/R_0 increase; it can be Slow (S) or Fast (F).
C5.3 Oscillation. The R/R_0 values oscillate around a certain mean value. The larger is the amplitude of oscillations, the larger AHE is.
C5.4 Constant. The R/R_0 not varying significantly over time. In this conditions AHE is absent.

We assume that these behaviors are closely correlated with a flux of the active species thorough the surface and/or bulk of the wire;

C6 Electric conditions of the counter-electrode, i.e. V, I, in DC or AC.
C7 AHE values (W), calculated using Eq. (1)(1–3). Maximum value measured was $+18$ W with 100 W input.
C8 Short comments on the experimental conditions and results.

Table 2. Summary of the most important operating conditions and results collected over two months of experiments.

C1 Test # *Timer (s)	C2 Wire, diameter (mm)	C3 *Pw_in (W) * V (V), I (A)	C4 Gas type, pressure (mbar)	C5 *T_core (°C); *R/R_0 wire; *loading variation	C6 Counter electrode, V, A; DC or 50 Hz AC (rms)	C7 AHE (W)	C8 Notes
#1 599280	0.350	40.6 19.5, 2.08	D_2 1810	318 0.885 DL_S		–0.7	10 July 2019. File started 03 July 2019, 16 h 44 m after several calibrations using nichrome and platinum heaters
#2 616410	0.350	60.6 24.1, 2.51	D_2 1770	427 0.905, DL_F		+8.7	Gas leak. Fast deuterium de-loading. Higher temperatures and fast unloading effective to get AHE
#3 691100	0.350	80.6 28.6, 2.8	D_2 1100	544 0.9524 DL_F		+7.8	Gas leak. Fast de-loading
#4 767700	0.350	97.4 31.6, 3.08	D_2 1100	630 0.964 DL_S		+0.5	Gas leak. Slow unloading. The *rate* of unloading is a key factor to get AHE.
#5 1005840	0.350	49.4, 22.2, 2.2	Ar/D_2= 1.34 1160	483 0.945 C		+0.2	R/R_0 almost constant. No AHE observed
#6 1015360	0.350	59.8, 24.6, 2.43	Ar/D_2= 1.34 1210	546 0.953 DL_F		+4.5	Fast unloading. AHE recovered
#7 1020670	0.350	70.2, 26.7, 2.62	Ar/D_2= 1.34 1230	603 0.961 IL_S		+2.8	Low speed loading, reduced AHE
#8 1029100	0.350	80.5, 28.7, 2.80	Ar/D_2= 1.34 1270	656 0.966 IL_S O		+8.6	Increasing loading, noisy R/R_0. The AHE increased largely, perhaps due to R/R_0 oscillations
#9 1037080	0.350	90.5, 30.6, 2.96	Ar/D_2= 1.34 1300	702 0.972 C O		+6.6	R/R_0 almost flat but with several instabilities. AHE present
#10 1097810	0.350	97.7, 31.7, 3.08	Ar/D_2= 1.34 1310	725 0.972 C O		+4.4	R/R_0 almost flat but with instabilities. Also the oscillations are useful to get AHE
#11 1340 New file			D_2 fresh 1960	22 0.926			Calorimeter opened and re-closed to repair a large gas leak. New file 170719_12:01
#12 18350	0.350	59.9, 24.4, 2.46	D_2 2610	420 0.906 IL_S		–0.5	In almost static conditions and high pressure no AHE, although some loading
#13 24230	0.200	60.4, 40,1.51	D_2 2440	439 0.949 IL_S O		+0.8	Gas leak. P_w at V2. Very slow loading. Some R/R_0 instability. Similar to test #12 but some weak oscill

Table 2 continued

#14 92900	0.200	60.1, 39.8, 1.51	D_2 2050	433 0.946 C	–0.7	Gas leak. 50 ks measurement. R/R_0 flat. No AHE
#15 172570	0.200	61.1, 40.1, 1.52	D_2 2610	438 0.947 C		Very long measures, 180 ks. R/R_0 flat. No AHE
#16 185120	0.200	80.5, 46.5,1.73	D_2 2670	529 0.962 C		Long duration measures. R/R_0 flat. No AHE
#17 195370	0.200	99.7, 52.1, 1.91	D_2 2710	607 0.977 DL_S O	+5.3	R/R_0 slowly increased. Some oscillations were the source of AHE
#18 196100	0.200	99.9, 52.2, 1.91	D_2 1970	611 0.978 O	*+10.1*	Forced pressure reduction. R/R_0 quite unstable: origin of AHE. *Short time test*
#19 196550	0.200	100.0, 52.3, 1.91	D_2 1470	617 0.978 DL_F O	*+9.7*	Forced pressure reduction. R/R_0 increased. *Short test*
#20 196960	0.200	100.0, 52.3, 1.91	D_2 1040	634 0.981 DL_F	*+7.7*	Forced pressure reduction. *No thermal equilibrium*
#21 197320	0.200	100.4; 52.4, 1.91	D_2 660	636 0.982 NA	*+6.0*	Forced pressure reduction. *No thermal equilibrium*
#22 198070	0.200	100.2; 52.5,1.91	D_2 440	659 0.986 NA	*+4.0*	Forced pressure reduction. *No thermal equilibrium*
#23 198600	0.200	100.6; 52.7, 1.91	D_2 300	685 0.990 NA	*+5.9*	Forced pressure reduction. *No thermal equilibrium*
#24 199160	0.200	100.2; 52.7, 1.90	D_2 196	713 0.995 NA	*+5.5*	Forced pressure reduction. *No thermal equilibrium*

Table 2 continued

#25 199860	0.200	99.9; 52.7, 1.89	D_2 156	733 0.997 NA		*+8.1*	Forced pressure reduction. *No thermal equilibrium*
#26 431190	0.200	81.2; 47.2, 1.72	D_2+ air 216	612 0.983 C		+0.5	Long measurement (>60 h). Leakage: air intake, initial 158 mbar at same temperatures. Some oscill.
#27 432920	0.200	81.2; 47.1, 1.72	D_2+ air 214	612 0.982 O	+300 V, 0.250 mA	+3.1	Counter electrode has positive Polarization: some AHE, at least at for short time.
#28 443190	0.200	81.1; 47.1, 1.72	D_2+ air 209	613 0.983 C	–300 V 0.210 mA	–2.1	Counter electrode Negative Polarization: AHE vanished, *even endothermic effects*
#29 451110	0.200	81.0; 47.1, 1.72	D_2+ air 218	614 0.983 C	–300 V 0.200 mA	–0.9	Pol. Neg. long time (>2 h). Slowly AHE endothermic region vanished
#30 598310	0.200	98.9; 52.1, 1.90	D_2+ air 330	688 0.983 IL_S		+1.7	Long measurement. Slow improvement of loading: some AHE
#31 77.7 616520	0.200	79.9; 46.5, 1.72	D_2+ air 270	596 0.969 C		+1.1	Leakage air intake observed. After an initial improvement, later R/R_0 flat
#32 620080	0.200	80.1; 46.6, 1.72	D_2+ air 184	609 0.972 O	±300 V 0.5–2 mA	+3.4	Forced pressure reduction. Several test with DC field P_{os}. and Neg. Indications that a change of polarity could be useful to get AHE
#33 623680	0.200	80.0; 46.6, 1.72	D_2+ air 211	613 0.973 O		+5.9	Abrupt temperature increase. DC field removed

Table 2 continued

#34 626380	0.200	80.2; 46.7, 1.72	D_2+ air 168	628 0.975 DL_S		+2.5	Forced pressure reduction
#35 630540	0.200	80.4; 46.8, 1.72	D_2+ air 187	631 0.976 DL_F	+296 V, 2.7 mA	+2.8	Pressure reduction and recovery. Fast increase R/R_0 DC field
#36 683800	0.200	80.7; 46.8, 1.72	D_2+ air 183	628 0.975 IL_S O	+296 V, 2.7 mA	+3.2	Long time with field. R/R_0 noisy. First time observed AHE not decreasing over time with power constant
#37 697670	0.200	89.7; 49.5, 1.81	D_2+ air 230	672 0.981 DL_F O	+297 V, 2 mA	+4.0	P_w increased from 80 to 90 W. Fast increase of R/R_0, oscillations of R/R_0
#38 716220	0.200	99.7; 52.3, 1.90	D_2+ air 300	716 0.985 DL_F O	+290 V, 3.2 mA	+18.0	P_w increased from 90 to 100 W. Fast increase of R/R_0. Osc. large AHE observed
#39 771310	0.200	99.7; 52.2, 1.91	D_2+ air 316	709 0.981 IL_S O	+297 V 3.15 mA	+9.5	Long duration 50 ks, at 100 W, DC field +300 V. R/R_0 decreased
#40 775060	0.200	99.6; 52.2, 1.91	D_2+ air 317	707 0.981 O	–297 V, –3.5 mA	+7.4	Test with negative field. Slowly decreasing AHE: Negative field effect
#41 789230	0.200	99.3; 52.1, 1.90	D_2+ air 341	706 0.981 O	AC, 260 V 2–3 mA	+10.7	AC stimulation, first time. RMS values. R_{equiv}: 100 kΩ. AHE recovered
#42 803300	0.200	100.2; 52.6, 1.90	D_2+ air 98	767 0.989 DL_F	AC, 260 V 2–3 mA	+14.5	Pressure reduced several times. AC on. Large R/R_0 increase

Table 2 continued

#43 1029400	0.200	99.2; 51.9, 1.91	D_2+ air 250	708 0.973 IL_S O		+2.4	Long time meas. Air intake: Press. increased. Temp. decreased. AHE decreased slowly. Loading Oscillations
#44 1032030	0.200	99.2; 51.9,1.91	D_2+ air 252	708 0.973 O	AC, 280 V 1–2 mA	+9.2	AC stimulation: recovered partially AHE, i.e. 2.4–9.2 W
#45 1114330	0.350	60.7; 24.7, 2.45	D_2+air 118	531 0.922 IL_S	AC, 260 V 5–6 mA	+0.2	Active wire 0.35 mm. First time
#46 1130570	0.350	79.8; 28.6, 2.79	D_2+air 163	634 0.934 DL_S	AC, 262 V 5 mA	–1.1	R/R_0slowly decreased. No AHE
#47 1143330	0.350	90.1; 30.4, 2.96	D_2+air 190	678 0.939 O	AC, 262 V 5 mA	+6.5	Several spikes at AC, R/R_0 noisy. Increasing P_w and temperature were useful
#48 1203690	0.350	60.4; 24.7, 2.45	D_2+air 104	539 0.921 DL_S	AC 260 V, 7 mA	+0.7	Regular oscillations. Weak AHE, although AC oscillation
#49 1215750	0.350	60.9; 24.9, 2.44	D_2+air 90	557 0.930 DL_S	AC, 263 V 5.8 mA	+0.9	Forced pressure reduction. No effect to recover AHE
#50 1219320	0.350	60.7; 24.8, 2.45	D_2+air 85	576 0.927 IL_S O	AC, 262 V 6.0 mA	+2.1	Forced pressure reduction. Increase of internal temperature and AHE
#51 1289670	0.200	61.2; 40.4, 1.51	Ar=D_2 87	575 0.956 O	AC, 293 V $\ll$1 mA	+3.1	After vacuum new gas (Ar=D_2 70 mbar at RT), Wire switch (V3 to V2). Smaller wire diameter, i.e. higher DC voltage, increased AHE
#52 1306580	0.200	80.15; 46.6,1.72	Ar=D_2 80	684 0.970 DL_S	AC, 293 V $\ll$1 mA	+2.2	Forced pressure reduction R/R_0 stable last 2 h

Table 2 continued

#53 1319520	0.200	100.1; 52.3, 1.91	Ar=D_2 90	770 0.980 DL_F O	AC, 293 V $\ll$1 mA	+9.1	Forced pressure reduction. AHE improved
#54 1321510	0.200	100.1; 52.4, 1.91	Ar=D_2 72	777 0.982 DL_S O	AC, 293 V $\ll$1 mA, self-pulse at HF	+11.3	Forced pressure reduction R/R noisy. Further increase of AHE. HF self-pulses look useful
#55 1370080	0.200	99.7; 52.0, 1.92	Ar=D_2 +air 125	734 0.974 IL_S	AC, 299 V $\ll$0.5 mA	+9.8	Leakage air intake. Several pressure reductions. AC current almost vanished Still AHE
#56 1374840	0.200	100.6; 52.5, 1.92	Ar= D_2 +air 45	799 0.982 D-I-L O	AC, 299 V $\ll$0.5 mA	+10.2	Several forced pressure reduction. AHE correlated with fast R/R_0 variation, oscill. high temperature
#57 1393640	0.200	99.5; 52.0, 1.91	Ar= D_2+air 94	750 0.974 O	AC, 299 V $\ll$0.5 mA	+8.7	Leakage air intake. Reducing local temperature decreases AHE
#58 1395760	0.200	101.3; 52.9, 1.92	Ar= D_2 +air 41	854 0.991 IL_F O	NO AC	+6	Forced pressure reduction. One of co-factor effects for AHE generation is AC stimulation, although HT increased (750–854)
#59 1403770 02/08/20 17:57	0.200	99.9; 52.2,1.91	Ar= D_2 + air 36	778 0.978 IL_F O	AC, 290 V 2–4 mA	+14.4	Forced pressure reduction. Large AHE. Geiger-Muller gamma detector several times in alarm ($\gg$4 BKG). R/R_0 decreased
#60 1447460	0.350	41.0; 20.3, 2.02	Ar= D_2 +air 66	510 0.917 C		–0.7	New file: 19082019, 13:37 Over 15 days operation at low power. No AHE
#61 1456770	0.350	41.1 20.4, 2.02	Ar= D_2+ air 30	547 0.924 DL_S	AC, 247 V 5.5 mA	+0.1	Reducing pressure and adding AC stimulation induced some AHE
#62 1461380	0.350	41.0 20.3, 2.01	Ar= D_2 + air 45	534 0.922 C	AC, 270 V 2–3 mA	–0.1	AC excitation ended 2 h before measurement. AHE vanished
#63 1522010	0.350	50; 22.5, 2.22	Ar= D_2 + air 57	582 0.926 DL_S	NO AC	–1.4	Without AC the weak AHE disappeared

Table 2 continued

#64 1549730	0.350	50; 22.5, 2.22	Ar= D_2+air 50	576 0.927 DL_S	AC, 247 V 4.9 mA	+0.6	Forced pressure reduction. AC field from 20 ks. No HF discharge. Weak AHE
#65 1554010	0.350	49.9; 22.5, 2.22	Ar= D_2+air 46	574 0.925 IL_S		+1.6	Pressure reduction. AC off since 1 h. R/R_0 decreased but AHE weak
#66 1610150	0.350	50; 22.5, 2.22	Ar= D_2+air 55	578 0.927 DL_S		–1.3	AC off since 16 h. Pressure increased, AHE vanished
#67 1627860	0.350	50; 22.3, 2.22	Ar= D_2+air 60	582 0.928 Osc.	AC, 290 V 1 mA	+1.5	AC field since 4 h R/R_0 noisy. Recovering of AHE
#68 1633300	0.350	50; 22.5, 2.22	Ar= D_2 +air 41	578 0.925 IL_S	NO AC	+0.1	Pressure reduced. AC stopped: AHE vanished.
#69 1640820	0.350	50.2; 22.6, 2.22	Ar= D_2 +air 20	600 0.930 IL_S Osc	AC, 290 V 1–2 mA	+2.6	Forced pressure reduction, AC ON since 2 h. AHE resumed
#70 1695500	0.350	60.5; 24.8, 2.43	Ar= D_2 +air 60	632 0.932 C		–1.8	NO AC. Pressure increased. R/R_0 stable; AHE absent
#71 1713770	0.350	60.5; 24.9, 2.43	Ar= D_2+air 30	660 0.936 IL_S	AC, 280 V 2–3 mA	+1.2	Forced pressure reduction. AHE improved
#72 1780200	0.350	80.1; 28.7, 2.79	Ar= D_2 +air 75	700 0.937 IL_S	AC, 253 V 4.5 mA. NO HF	–1.3	AC seems NOT effective to stimulate AHE without HF component
#73 1787240	0.350	80.0; 28.6, 2.79	Ar= D_2 +air 85	692 0.937 IL_F O	AC, 253 V 4.5 mA. Some HF	+3.2	AC ON, sometimes HF. R/R_0 noisy
#74 1806940	0.350	97.8; 31.7, 3.08	Ar= D_2+ air 150	757 0.942 IL_F O		+4.8	R/R_0 decreasing. Absolute value of local high temperature (760°C) is also important
#75 1812230	0.350	98.2 31.9, 3.08	Ar= D_2 62	802 0.946 IL_F O	AC, 260 V 4 mA	+7	AC ON, some spontaneous HF. Forced pressure reduction. Combined effect of higher temperature, low pressure-AC excitation is

Table 2 continued

#76 2043780	0.350	97.4 31.6, 3.08	Ar= D_2 +air 146	719 0.935 IL_S	AC, 290 V <1 mA	+2.8	AC ON, leakage air intake. AHE reduction (7.2–2.8) because: pressure increasing, lower AC, lower temperature
#77 76650 New file 260827, 11:27	0.350	40.6; 20.1, 2.02	D_2 fresh 440	336 0.906 IL_S O	AC, 290 V 1–2 mA	+1.8	After vacuum, fresh D_2 (380 mbar at RT). Increasing of loading. Noisy. Some AHE, although low power and temperature. Flux of D_2 looks important
#78 26480 New file 270819, 10:18	0.200	40.5; 32.4, 1.25	D_2, 480	463 0.929 IL_S	AC, 300 V <0.5 mA NO HF	–0.3	Re-activated V2. Slow loading speed. No AHE, although AC oscillation but no HF components. Pressure excessive and temperature not sufficient for AHE
#79 37570	0.200	60.7; 40.1, 1.51	$D_2$15	580 0.959 O	AC, 290 V <0.6 mA	+4.9	Forced pressure reduction. R/R_0 noisy: combined effects with HT. AHE resumed
#80 89.1 116590	0.200	81.5; 47.0, 1.73	$D_2$26	720 0.971 IL_F Osc.	AC, 290 V 0.3–1 mA	+115	Forced pressure reduction. R/R_0 noisy and decreasing. HT, low pressure, oscill.: ingredients to get AHE
#81 174740	0.200	81.2; 46.7, 1.73	D_2+air 34	691 0.964 IL_F O	AC, 290 V 0.4 mA	+8.3	AC polarization started. Leakage, air intake observed. Reduction of temperature decreases AHE (11.5–8.3)
#82 195640	0.200	100.4; 52.2, 1.92	D_2+ air 75	764 0.970 IL_F O	AC, 290 V 0.2–1 mA	+13.0	AC always active. R/R_0 noisy and decreasing fast. The AC keeps AHE stable over time
#83 204780	0.200	101; 52.6, 1.92	D_2+air 30	808 0.981 IL_F O	AC, 290 V 0.2–1 mA	+12.8	Several pressure reduction steps. AC always active. R/R_0 noisy and decreasing. Although air intake AHE almost stable

Table 2 continued

#84 257660	0.200	100.3; 52.1, 1.92	D_2+air 50	753 0.97 IL_F Osc.	AC, 290 V 0.2–0.5 mA	+11.2	Long duration measures. AC ON. Leakage and air intake occurred. R/R_0 noisy and decreasing. The combined effect of high temperature, AC oscillation and sufficiently low pressure overcome the deleterious effect of air intake even for long times (>14 h). *Last measurement before ICCF22*

Addendum

(1) After the ICCF22 conference we received enquiries whether we have a theory supporting the correlation between AHE occurrence and electron emission. Unfortunately to date we can only speculate that electron emission may cause D+ ions in gaseous phase to move toward the surface of the Constantan wire, possibly contributing to the D flux or inducing extreme localized gradients beneficial to the manifestation of AHE (especially on the nanostructures present on the surface of the wire).

(2) The gamma source contains 10 g of ^{232}Th in form of Thoriated Tungsten (i.e. electrodes used for TIG welding). Thorium is dispersed at 2% concentration w/w in a matrix of W. The specific activity of ^{232}Th is 4.07 $\times 10^3$ Bq/g, mostly alpha and beta radiations. In addition there are several gamma, even at high energies (2614 keV), due to his decay products (^{228}Ac, ^{212} Bi, ^{212}Pb, ^{212}Po, ^{224}Ra, ^{228}Ra, and ^{208}Tl). The tube were the material is inserted is a 2 mm tick stainless steel tube, hermetically closed. In short, the measured gamma activity, measured using just a simple Geiger Muller detector, is over 10 times larger of local background (35–40 μRem/h). Moreover, a 3×3 inch NaI(Tl) detector was successfully used to identify the ^{232}Th gamma peaks up to 2 MeV of energy.